Geophysical Research Letters

RESEARCH LETTER
10.1029/2019GL083341

OSIRIS-REx Visible and Near-Infrared Observations of the Moon

A. A. Simon[1], K. L. Donaldson Hanna[2,3], C. Y. Drouet d'Aubigny[4], G. Poggiali[5,6], J. P. Emery[7], J. Brucato[5], R. G. Cosentino[8], D. C. Reuter[1], D. R. Golish[4], D. N. DellaGiustina[4], A. Lunsford[9], N. Gorius[10], P. H. Smith[4], and D. S. Lauretta[4]

[1]NASA Goddard Space Flight Center, Greenbelt, MD, USA, [2]Department of Physics, Oxford University, Oxford, UK, [3]Department of Physics, University of Central Florida, Orlando, FL, USA, [4]Lunar and Planetary Laboratory, University of Arizona, Tucson, AZ, USA, [5]INAF-Osservatorio Astrofisico di Arcetri, Florence, Italy, [6]Department of Physics and Astronomy, University of Florence, Florence, Italy, [7]Department of Earth and Planetary Sciences, University of Tennessee Knoxville, Knoxville, TN, USA, [8]Astronomy Department, University of Maryland College Park, College Park, MD, USA, [9]Physics Department, American University, Washington, DC, USA, [10]Department of Physics, Catholic University, Washington, DC, USA

Key Points:
- The OSIRIS-REx mission obtained observations of Earth and the Moon during a 2017 gravity assist maneuver
- Visible and near-infrared spectra of the Moon show features consistent with plagioclase-dominated mixtures expected in highlands terrain
- The 2.8-μm hydration band is observed in full-disk spectra, confirming previous spacecraft observations

Correspondence to:
A. A. Simon,
amy.simon@nasa.gov

Citation:
Simon, A. A., Donaldson Hanna, K. L., Drouet d'Aubigny, C. Y., Poggiali, G., Emery, J. P., Brucato, J., et al. (2019). OSIRIS-REx visible and near-infrared observations of the Moon. *Geophysical Research Letters*, *46*, 6322–6326. https://doi.org/10.1029/2019GL083341

Received 15 APR 2019
Accepted 3 JUN 2019
Accepted article online 6 JUN 2019
Published online 19 JUN 2019

Abstract The Origins, Spectral Interpretation, Resource Identification, and Security-Regolith Explorer (OSIRIS-REx) mission observed the Moon during the spacecraft's Earth gravity assist in 2017. From the spacecraft view, the lunar phase was 42°, and the in-view hemisphere was dominated by anorthositic highlands terrain. Lunar spectra obtained by the OSIRIS-REx Visible and InfraRed Spectrometer show evidence of several candidate absorption features. We observe the 2.8-μm hydration band, confirming the spectral results from other missions, but detected in full-disk spectra. We also tentatively identify weak spectral features near 0.9 and 1.3 μm, consistent with lunar regolith containing a mixture of plagioclase and orthopyroxene minerals, as expected for highlands terrain.

Plain Language Summary: The Origins, Spectral Interpretation, Resource Identification, and Security-Regolith Explorer mission obtained observations of Earth and the Moon during a 2017 gravity assist maneuver. The Origins, Spectral Interpretation, Resource Identification, and Security-Regolith Explorer Visible and InfraRed Spectrometer acquired several spectra that covered the fully illuminated portion of the Moon. These spectra show absorption features consistent with the mineral mixtures expected in the lunar Highlands terrains. Near-simultaneous images show that the side of the Moon that was visible is dominated by this type of terrain. In addition, an infrared absorption, consistent with water-bearing minerals, is also observed, confirming the spectral identifications made by previous missions that have observed the Moon.

1. Introduction

The Origins, Spectral Interpretation, Resource Identification, and Security-Regolith Explorer (OSIRIS-REx) spacecraft flew by the Earth-Moon system in 2017, completing a gravity assist en route to the asteroid (101955) Bennu (Lauretta et al., 2017). This flyby gave an opportunity for testing operational scenarios and confirming instrument calibration. It also allowed for science observations of Earth and the Moon by the OSIRIS-REx Visible and InfraRed Spectrometer (OVIRS). OVIRS produces point spectra of a 4-mrad circular field of view (FOV) using five linear variable filters from 0.4 to 4.3 μm and was designed to detect spectral absorption features down to 2.5% band depth (Reuter et al., 2018). The Moon was observed on 25 September, when it partially filled the OVIRS aperture. Although the Moon was only partially illuminated, sufficient signal was obtained to produce spectra that can be compared with observations from previous missions, including EPOXI, Chandrayaan, and Cassini.

2. Observations

On 25 September 2017, three days after OSIRIS-REx completed its Earth gravity assist, the spacecraft executed four east-west and four north-south scans across the Moon from a distance of 1.166×10^6 km. The scans were designed to provide overlap in the OVIRS FOV with 2-mrad lateral separation between scans

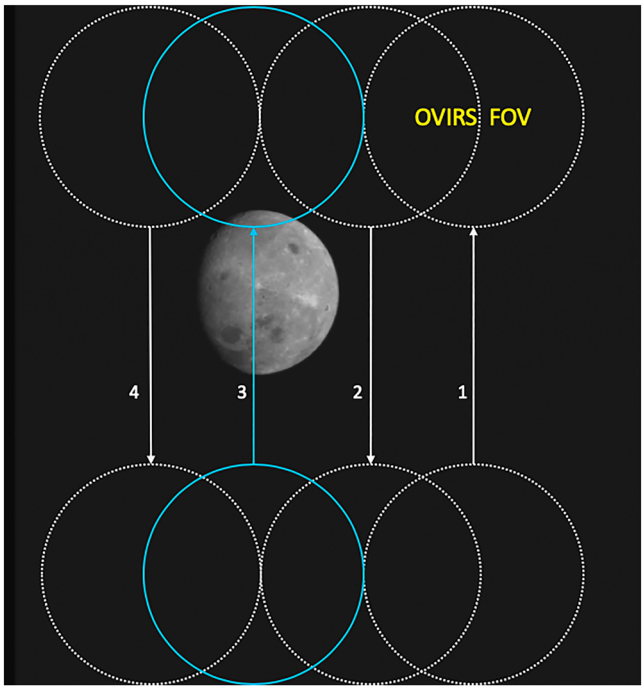

Figure 1. Origins, Spectral Interpretation, Resource Identification, and Security-Regolith Explorer Visible and InfraRed Spectrometer (OVIRS) scans of the Moon. The approximate geometry during the lunar observation is shown, with an OVIRS field of view (FOV) overlain on a near-simultaneous panchromatic image from the Origins, Spectral Interpretation, Resource Identification, and Security-Regolith Explorer Camera Suite. The blue circles indicate the scan that crossed the Moon.

(Figure 1). At this distance, the Moon subtended 3 mrad, and the maximum possible OVIRS area fill factor was ~0.56. The phase angle was 42.3°, so the lunar disk was not fully illuminated.

As these scans were designed, in part, to determine the absolute pointing of the spectrometers, the OVIRS FOV scanned rapidly across the Moon and surrounding area. Most scans have no lunar signal, and only a few spectra from the eight scans show full signal equivalent to the 0.56 fill factor. We chose the two best spectra (those with the maximum fill factor) and averaged them for all subsequent analyses (Reuter et al., 2019). Because the pointing changed throughout a scan, the two adjacent spectra had slightly different geometries, giving an average subspacecraft latitude and longitude of 21.4° and 122°, respectively. A near-simultaneous image by the OSIRIS-REx Camera Suite shows the portion of the lunar surface that was visible and illuminated (Figure 1).

3. Analyses

All OVIRS spectra pass through an automatic calibration pipeline to convert from raw counts to physical radiance units (W/cm^2/sr/μm), following the method described in Simon et al. (2018). The ground testing-derived radiometric calibration and out-of-band removal coefficients were adjusted after the Earth gravity assist and again on approach to (101955) Bennu. The lunar data were then recalibrated using these latest Bennu-approach calibration files to produce the average radiance spectrum. Out-of-band (IR signal in all shorter wavelength filters) leakage is corrected using OVIRS ground calibration data of single temperature blackbody sources with a wavelength-independent emissivity of 0.992 (Simon et al., 2018). The correction assumes only the sum of 2.8 to 3.95-μm photons contribute to the out-of-band signal, with a linear response at wavelengths below 2.8 μm only dependent on blackbody temperature. Thus, observed sources with a more complex IR signature do not completely correct, and this effect generally appears on the short wavelength ends of the filters, (i.e., 1.7, 1.07, .66, and.4 μm). Although obvious residual out-of-band signal is a small contribution (<1%) in the lunar spectra, it was corrected by finding each filter's average radiance at short wavelengths where it overlapped with the next filter and removing a linear slope to align them. This results in a corrected average radiance (Figure 2, top); there is still some radiometric calibration uncertainty in the 2- to 3-μm region where the Bennu and Earth signals are lowest.

To determine reflectance, we first subtracted a thermal tail from the radiance (Figure 2, blue curve). Owing to the phase angle and full-disk view, multiple surface temperatures are present in the FOV, but the highest temperature locations will have the largest radiance and dominate the thermal emission. The thermal tail was simulated by fitting the long wavelength radiance spectrum using a single blackbody temperature and wavelength-independent emissivity, ε. This results in a best fit blackbody temperature of 382.5 K with $\varepsilon = 0.167$. Given the local time of day, this is not an unreasonable maximum temperature (Williams et al., 2017). The very low emissivity reflects the fact that most of the visible surface is much cooler and acts as a temperature fill factor of sorts. The reflectance is then calculated by dividing the thermal-subtracted radiance by a phase angle-scaled solar spectrum and adjusting it for the FOV fill factor. To correct for phase angle, we used a wavelength-independent limb darkening factor of 0.019 magnitudes per degree (McEwen, 1996), which gives a reflectance adjustment of ~0.48, in rough agreement with Hapke et al. (2012). Finally, we smoothed any remaining noise using a 5-point running mean (Figure 2, bottom, black line).

The resulting reflectance values are approximately consistent with the Apollo 16 lunar soils, and anorthositic highlands terrain, which dominate the illuminated portion of the surface in Figure 1 (e.g., Kieffer & Stone, 2005; Ohtake et al., 2009; Pieters, 1999). The global reflectance spectrum shows a distinct absorption feature, the 2.8-μm hydration band, consistent with O-H and water-bearing minerals (e.g., Clark, 2009; Sunshine et al., 2009). The approximate band depth is indicated by the gray area in Figure 2 (bottom),

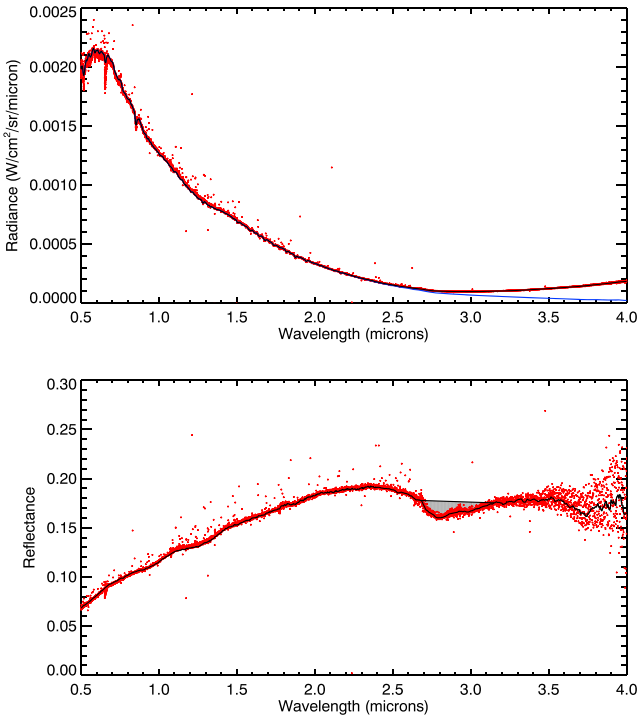

Figure 2. Origins, Spectral Interpretation, Resource Identification, and Security-Regolith Explorer Visible and InfraRed Spectrometer average lunar spectrum from 0.5 to 4.0 μm. Top, radiance spectrum showing each pixel (red points) and overlain with the resampled spectrum (spectral resolution of 2 nm at wavelengths <2.4 μm and 5 nm at wavelengths from 2.4 to 4.0 μm; outlying bad pixels removed; black curve). A thermal tail (blue curve) is removed for all subsequent analyses. Bottom, reflectance spectrum from each pixel (red points) and from resampled radiance, smoothed with a 5-point running mean (black curve). The gray area indicates the 2.8-μm hydration feature from 2.68 to 3.15 μm.

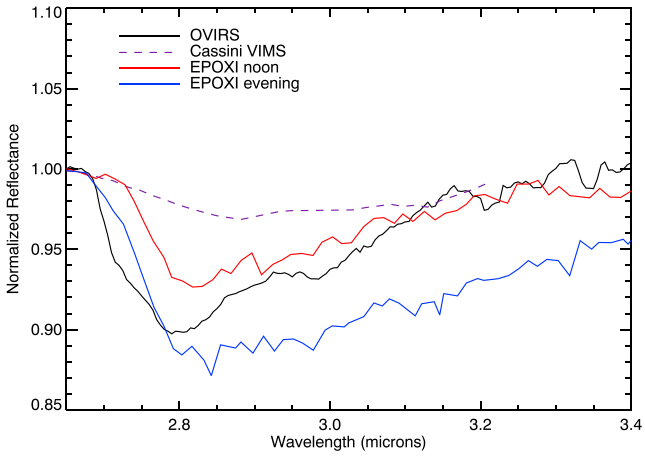

Figure 3. Origins, Spectral Interpretation, Resource Identification, and Security-Regolith Explorer Visible and InfraRed Spectrometer (OVIRS) hydration feature band depth, normalized at 2.65 μm. The OVIRS curve (black) agrees well with EPOXI-normalized spectra of the lunar highlands (red and blue), both of which are deeper than Cassini Visible and Infrared Mapping Spectrometer (VIMS) data (dashed purple line; from Clark, 2009, spectrum S6).

using the same wavelength tie points for the continuum as Clark (2009). The larger scatter in the OVIRS data at 2.85 to 2.95 μm is where filter segments overlap and is probably due to uncorrected out-of-band effects.

4. Discussion

We can rule out any internal instrument contamination as a source of the observed band, as decontamination heaters were used between launch and the Earth encounter to drive off any residual water condensation. Additionally, internal instrument calibration sources were observed during thermal vacuum testing after a hot bake out (50 °C) and during cruise to show no instrument performance changes have occurred in this wavelength region. The internal blackbody sources, in particular, show no evidence of a 2.8-μm absorption band.

To compare the full-disk 2.8-μm band depth with prior spacecraft observations, we normalized the reflectance spectrum to the reflectance at 2.65 μm (Figure 3). From this, we can estimate the band depth at 2.8 μm, as in Sunshine et al. (2009). We find a 2.8-μm band depth of 10 ± 2%, consistent with Deep Impact/EPOXI spectra of both maria and highlands at afternoon local time locations (Sunshine et al., 2009). This band depth is larger than what Clark (2009) found in polar and highlands spectra (~4%) obtained by the Cassini Visible and Infrared Mapping Spectrometer. Similar studies of Chandrayaan-1 Moon Mineralogy Mapper (M^3) data initially found absorptions only near the poles (Pieters et al., 2009). Subsequent analyses showed that with better thermal tail subtraction, the 2.8-μm absorption band was visible to M^3 in other regions as well but the band depth could not be calculated owing to the spectral range (Clark et al., 2010). In the OVIRS spectra, the thermal tail shape removal is likely imperfect, because of the multiple surface temperature in the FOV, and we cannot interpret the band shape differences as meaningful. However, the band depth is most consistent with the M3 and EPOXI data, perhaps due to the hemisphere that was observed or differing viewing geometry, including local time of day (Clark, 2009). Additionally, residual calibration issues may mean the OVIRS band is actually slightly shallower than seen in Figure 3.

Typical spectra of lunar rocks and regolith as well as remote sensing observations of the lunar surface include diagnostic mineral bands of pyroxene, plagioclase, and olivine (e.g., Pieters, 1986). To check for these signatures, we divided the reflectance by a smoothed continuum (using a quadratic fit; Figure 4, top). We observe two potential features near 0.9 and 1.3 μm, consistent with mixtures of plagioclase (the most abundant mineral in anorthositic rocks) and orthopyroxene (Cheek & Pieters, 2014). This spectral signature is similar to M^3 observations of a number of lunar locations, including Orientale Basin's Inner Rook ring and the Aristarchus, Tsiolkovskiy, and Langrenus craters, which have also been identified as anorthositic materials with varying amounts of plagioclase and orthopyroxene (e.g., Cheek & Pieters, 2014; Donaldson Hanna et al., 2014; Horgan et al., 2014). Comparing with Kaguya Spectral Profiler data, the OVIRS spectra are similar to Feldspathic Highlands Terrane spectra, though the Spectral Profiler data have a deeper absorption around 0.9 μm and a shallower absorption shoulder around 1.25 μm (Lucey et al., 2014).

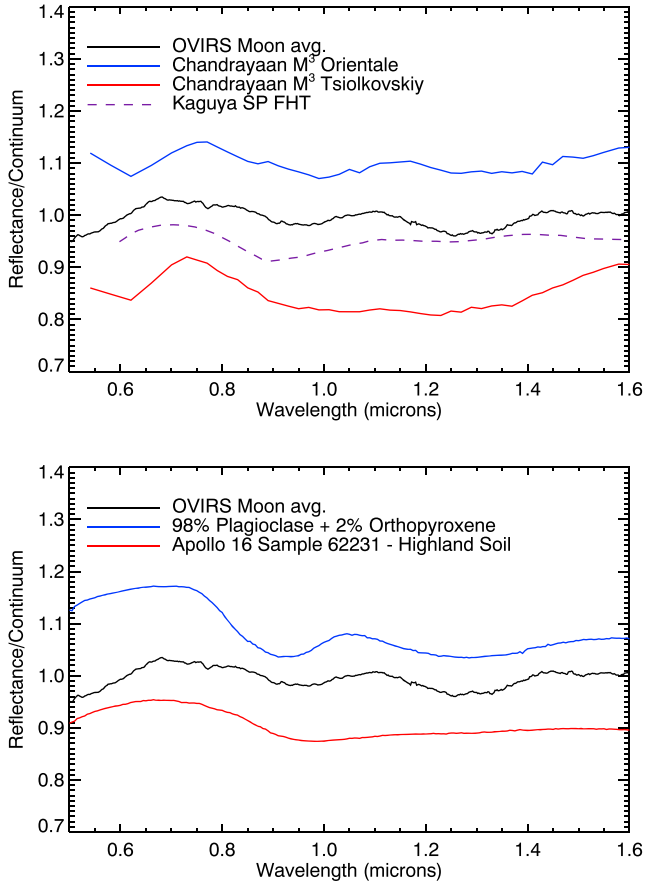

Figure 4. Origins, Spectral Interpretation, Resource Identification, and Security-Regolith Explorer Visible and InfraRed Spectrometer (OVIRS) continuum-divided reflectance spectrum. Top, comparison of OVIRS spectrum with Chandrayaan M^3 data, reproduced from Cheek and Pieters (2014), and Kaguya Spectral Profiler (SP) data, reproduced from Lucey et al. (2014). Bottom, comparison of OVIRS spectrum with laboratory data of Apollo 16 bulk soil (Pieters, 1986) and mineral mixtures (Cheek & Pieters, 2014). FHT = Feldspathic Highlands Terrane.

The OVIRS lunar spectrum shows an approximately 3% band depth in the 0.9-μm orthopyroxene band and 5% in the 1.3-μm plagioclase feldspar band. As shown in Figure 4 (bottom), this is a very good match with laboratory spectra containing 98% plagioclase and 2% orthopyroxene (Cheek & Pieters, 2014). Apollo 16 soil samples also show absorption near 0.9 μm, though none at 1.3 μm. We interpret the OVIRS spectrum as consistent with anorthositic rock, and highlands terrain, in good agreement with Lucey et al.'s (2014) map of this region.

5. Summary

During the OSIRIS-REx Earth-Moon flyby in 2017, OVIRS collected lunar spectra that show evidence of several candidate spectral features. The 2.8-μm hydration band is observed in full-disk spectra for the first time and is consistent with near-IR spectral results from Cassini, EPOXI, and Chandrayaan-1. This confirms the previous detections, while also validating our thermal tail subtraction method. The full-disk detection of this feature is likely due to the hemisphere that was viewed, which is dominated by the anorthositic highlands terrain where this absorption is most often observed. We additionally identify shallow spectral features near 0.9 and 1.3 μm, with 3% and 5% band depths, respectively, confirming OVIRS' ability to detect weak absorption bands. These features also consistent with regolith materials that include a mixture of plagioclase and orthopyroxene minerals. At Bennu, the OVIRS-optimized compositional observations occur at lower phase angles and with cooler predicted surface temperatures, which maximizes the signal while minimizing the thermal contribution. Based on the analysis techniques and sensitivity demonstrated with the lunar data, we expect to be able to map compositional variations on Bennu's surface in fine detail.

Acknowledgments

We are grateful to the entire OSIRIS-REx Team for making the encounter with Earth possible, particularly the efforts of the operations and navigations teams. All data may be obtained through the Small Bodies Node of the Planetary Data System (https://sbn.psi.edu/pds/resource/orex/). This material is based upon work supported by NASA under Contract NNM10AA11C issued through the New Frontiers Program INAF participation that was supported by the Italian Space Agency Grant Agreement 2017-37-H.0. The authors declare no competing financial interests.

References

Cheek, L. C., & Pieters, C. M. (2014). Reflectance spectroscopy of plagioclase-dominated mineral mixtures: Implications for characterizing lunar anorthosites remotely. *American Mineralogist*, *99*, 1871–1892. https://doi.org/10.2138/am-2014-4785

Clark, R., Pieters, C. M., Green, R. O., Boardman, J., Buratti, B., Head, J. W. et al. (2010). Water and hydroxyl on the Moon as seen by the Moon mineralogy mapper (M3). LPI Contribution No. 1533, p. 2302.

Clark, R. N. (2009). Detection of adsorbed water and hydroxyl on the Moon. *Science*, *326*, 562–564. https://doi.org/10.1126/science.1178105

Donaldson Hanna, K. L., Cheek, L. C., Pieters, C. M., Mustard, J. F., Greenhagen, B. T., Thomas, I. R., & Bowles, N. E. (2014). Global assessment of pure crystalline plagioclase across the Moon and implications for the evolution of the primary crust. *Journal of Geophysical Research: Planets*, *119*, 1516–1545. https://doi.org/10.1002/2013JE004476

Hapke, B., Denevi, B., Sato, H., Braden, S., & Robinson, M. (2012). The wavelength dependence of the lunar phase curve as seen by the Lunar Reconnaissance Orbiter wide-angle camera. *Journal of Geophysical Research*, *117*, E00H15. https://doi.org/10.1029/2011JE003916

Horgan, B. H. N., Cloutis, E. A., Mann, P., & Bell, J. F. III (2014). Near-infrared spectra of ferrous mineral mixtures and methods for their identification in planetary surface spectra. *Icarus*, *234*, 132–154. https://doi.org/10.1016/j.icarus.2014.02.031

Kieffer, H. H., & Stone, T. C. (2005). The spectral irradiance of the Moon. *Astronomical Journal*, *129*, 2887–2901.

Lauretta, D. S., Balram-Knutson, S. S., Beshore, E., Boynton, W. V., Drouet d'Aubigny, C., DellaGiustina, D. N., et al. (2017). OSIRIS-REx: Sample return from asteroid (101955) Bennu. *Space Science Reviews*, *212*(1-2), 925–984. https://doi.org/10.1007/s11214-017-0405-1

Lucey, P. G., Norman, J. A., Crites, S. T., Taylor, G. J., Hawke, B. R., Lemelin, M., & Melosh, H. J. (2014). A large spectral survey of small lunar craters: Implications for the composition of the lunar mantle. *American Mineralogist*, *99*, 2251–2257. https://doi.org/10.2138/am-2014-4854

McEwen, A. S. (1996). A precise lunar photometric function. *Lunar and Planetary Science* 27, p. 841.

Ohtake, M., Matsunaga, M. T., Haruyama, J., Yokota, Y., Morota, T., Honda, C., et al. (2009). The global distribution of pure anorthosite on the Moon. *Nature*, *461*(7261), 236–240. https://doi.org/10.1038/nature08317

Pieters, C. M. (1986). Composition of the lunar highland crust from near-infrared spectroscopy. *Reviews of Geophysics*, *24*, 557–578.

Pieters, C. M. (1999). In L. Gaddis & C. K. Shearer (Eds.), *New Views of the Moon II: Understanding the Moon through the integration of diverse datasets* (p. 47, Abstract #8025). Houston: LPI.

Pieters, C. M., Goswami, J. N., Clark, R. N., Annadurai, M., Boardman, J., Buratti, B., et al. (2009). Character and spatial distribution of OH/H2O on the surface of the Moon seen by M^3 on Chandrayaan-1. *Science*, *326*(5952), 568–572. https://doi.org/10.1126/science.1178658

Reuter, D. C., Simon, A. A., Hair, J., Lunsford, A., Manthripragada, S., Bly, V., et al. (2018). The OSIRIS-REx Visible and InfraRed Spectrometer (OVIRS): Spectral maps of the asteroid Bennu. *Space Science Reviews*, *214*(2), 54. https://doi.org/10.1007/s11214-018-0482-9

Reuter, D. C., A. A. Simon, A. Lunsford, D. S. Lauretta (2019). Origins, Spectral Interpretation, Resource Identification, Security, Regolith Explorer (OSIRIS-REx): Visible and InfraRed Spectrometer (OVIRS) bundle, urn:nasa:pds:orex.ovirs, NASA Planetary Data System.

Simon, A. A., Reuter, D. C., Gorius, N., Lunsford, A., Cosentino, R. G., Wind, G., Lauretta, D., & the OSIRIS-REx team (2018). In-flight calibration and performance of the OSIRIS-REx Visible and IR Spectrometer (OVIRS). *Remote Sensing*, *10*, 1486. https://doi.org/10.3390/rs10091486

Sunshine, J. M., Farnham, T. L., Feaga, L. M., Groussin, O., Merlin, F., Milliken, R. E., & A'Hearn, M. F. (2009). Temporal and spatial variability of lunar hydration as observed by the Deep Impact spacecraft. *Science*, *326*, 565–568. https://doi.org/10.1126/science.1179788

Williams, J.-P., Paige, D. A., Greenhagen, B. T., & Sefton-Nash, E. (2017). The global surface temperatures of the Moon as measured by the Diviner Lunar Radiometer Experiment. *Icarus*, *283*, 300–325. https://doi.org/10.1016/j.icarus.2016.08.012